OPEN ACCESS

University of BRISTOL

Qiao, Y., Li, M., Booth, R., & Mann, S. (2017). Predatory behaviour in synthetic protocell communities. Nature Chemistry, 9(2), 110-119. DOI: 10.1038/NCHEM.2617

Peer reviewed version

Link to published version (if available):
10.1038/NCHEM.2617

Link to publication record in Explore Bristol Research
PDF-document

University of Bristol - Explore Bristol Research
General rights

Predatory behaviour in synthetic protocell communities

Yan Qiao, Mei Li, Richard Booth and Stephen Mann[*]

Centre for Protolife Research and Centre for Organized Matter Chemistry, School of Chemistry, University of Bristol, Bristol BS8 1TS, United Kingdom
*email: s.mann@bristol.ac.uk

Recent progress in the chemical construction of colloidal objects comprising integrated biomimetic functions is paving the way towards rudimentary forms of artificial cell-like entities (protocells). Although several new types of protocells are currently available, the design of synthetic protocell communities and investigation of their collective behaviour has received little attention. Here we demonstrate an artificial form of predatory behaviour in a community of protease-containing coacervate micro-droplets and protein-polymer microcapsules (proteinosomes) that interact via electrostatic binding. The coacervate micro-droplets act as killer protocells for the obliteration of the target proteinosome population by protease-induced lysis of the protein-polymer membrane. As a consequence, the proteinosome payload (dextran, *ss*-DNA, platinum nanoparticles) is trafficked into the attached coacervate micro-droplets, which are then released as functionally modified killer protocells capable of re-killing. Our results highlight opportunities for the development of interacting artificial protocell communities, and provide a strategy for inducing collective behaviour in soft matter micro-compartmentalized systems and synthetic protocell consortia.

Introduction

The design and construction of compartmentalized colloids that exhibit biomimetic properties such as membrane gating, molecular crowding, spatially controlled reactivity and information processing is providing new approaches to the fabrication of small-scale objects with integrated materials functions[1-3] and synthetic cell-like behaviours (protocells).[4-6] Examples of protocells include lipid[7,8] and polymer[9,10] vesicles, lipid vesicles containing discrete polymer-enriched internalized domains,[11,12] layer-by-layer microcapsules of counter-charged polyelectrolytes,[13,14] surfactant-stabilized water-in-oil emulsions,[15,16] inorganic nanoparticle-stabilized colloidosomes,[17] cross-linked shells of protein-polymer nano-conjugates (proteinosomes),[1,18] membrane-free liquid micro-droplets prepared by complex coacervation,[19] and membrane-coated coacervate micro-droplets with sub-divided[20,21] or homogenous[22] interiors. Integration of various functional components into these self-assembled micro-architectures under close to equilibrium conditions has been exploited to generate various minimal representations of synthetic cellularity. For example, selective membrane permeability, guest molecule encapsulation, gene-directed protein synthesis, membrane-gated enzyme activity, and membrane-mediated tandem catalysis have been demonstrated in proteinosomes.[1,18,23]

Similarly, coacervate micro-droplets are currently being investigated as membrane-free artificial cellular platforms due to their propensity to sequester a wide range of biological molecules and machinery,[19,24,25] exhibit enhanced enzymatic activity,[26] and undergo electric field-induced energization under non-equilibrium conditions.[27]

Taken together, the above investigations exemplify a modern approach to synthetic cellularity that advances the physical and chemical basis of cell structure and function,[28,29] and provides steps towards new colloid-based technologies geared towards the development of smart autonomously functioning chemical micro-compartments.[30,31] To date, the focus has been primarily on the construction of integrated components and networks within individual protocell constructs; in contrast, the design of synthetic protocell communities and investigation of their collective behaviour has received much less attention, even though a range of different protocell types are now available and preparing consortia of these compartmentalized microscale objects is readily accessible. Within this context, recent studies have demonstrated chemical communication and unidirectional signalling pathways between populations of synthetic vesicles and bacterial cells via carbohydrate-[32] or riboswitch-induced mechanisms,[33] amongst a dispersion of water-in-oil emulsion droplets filled with an *in vitro* transcriptional oscillator,[34] along linear chains of water-in-oil emulsion droplets containing either bacteria or a cell-free gene expression system,[35] between membrane-coated coacervate micro-droplets containing single components of a two-step enzyme cascade reaction,[21] and within a binary population of colloidosomes connected via an enzyme-induced hydrogen peroxide switch.[36] Such studies suggest that protocell networks could have potential as consortia for use as multiplex micro-reactor networks in areas such as biomimetic systems engineering and synergistic sensing systems.[37]

Although rudimentary in design, communities of protocells provide an opportunity to develop functional colloidal systems capable of collective behaviour, population dynamics and adaptation to changes in their external environment – a form of *protocell ecosystem* so to speak. In this paper, we address the challenge of how to design interacting protocell communities exhibiting a simple form of predatory behaviour in which a population of "killer" ("predator") coacervate-based protocells seeks out and obliterates a coexisting population of "target" ("prey") proteinosome-based protocells. The killing process is established by chemically charging the coacervate micro-droplets with a protease that promotes lysis of the protein-polymer membrane of the proteinosomes only when the two different types of

protocells come into contact via electrostatic interactions associated with opposite surface charges. Moreover, the propensity of the coacervate droplets to strongly sequester a wide range of molecular and macromolecular solutes[19] enables the killer protocells to mediate the extraction, transfer and subsequent capture of various payloads housed within the target protocells to generate a primitive form of inter-protocellular trafficking of functional components. We use cell sorting techniques to determine the population dynamics in these synthetic protocell communities, and optical and fluorescence microscopy to elucidate the mechanisms responsible for the apparent predatory behaviour as well as the trafficking of polysaccharides, genetic polymers and platinum nanoparticles from the proteinosomes to the coacervate micro-droplets during the killing process.

Results and discussion

Design and construction of a synthetic predator-prey protocell community. Artificial communities of interacting synthetic protocells exhibiting a rudimentary form of predatory behaviour were established by mixing aqueous dispersions of positively charged protease K-sequestered poly(diallyldimethylammonium chloride) (PDDA)/adenosine 5$^/$-triphosphate (ATP) coacervate micro-droplets[19] and negatively charged bovine serum albumin (BSA-NH$_2$)/poly(N-isopropylacrylamide) (PNIPAAm) proteinosomes[18] containing FITC-labeled dextran or ssDNA (Fig. 1a). The coacervate dispersions were prepared in the presence of protease K at an initial PDDA : ATP monomer mole ratio of 1 : 1, and then centrifuged and re-dispersed in Milli-Q water to produce suspensions of positively charged membrane-free micro-droplets (zeta potential (ζ), *ca.* + 30 mV (Supplementary Fig. 1a) containing the sequestered enzyme. In contrast, the proteinosomes were negatively charged (zeta potential, ca. -10 mV; Supplementary Fig. 1b), and consisted of a semi-permeable nanometer-thin membrane of covalently cross-linked protein-polymer nanoconjugates[18] surrounding an aqueous lumen containing a payload of encapsulated polysaccharide or polynucleotide molecules. Optical and fluorescence microscopy images of the FITC-labeled enzyme-containing coacervate suspensions showed discrete spherical micro-droplets that exhibited high optical contrast and green fluorescence intensity (Fig. 1b,c and Supplementary Fig. 2a,b), and were less than 15 μm in diameter (mean size, 2 μm (Supplementary Fig. 2c)). Uptake of FITC-protease K appeared homogeneous throughout the coacervate micro-droplets with no evidence for surface localization or internal aggregation,

suggesting that the enzyme was uniformly partitioned into the liquid micro-compartments. Determination of the protease K equilibrium partition coefficient (K = [protease K]$_{in}$/[protease K]$_{out}$) gave a value of 350 (see Methods), which corresponded to a concentration of ca. 12 μM within the molecularly crowded environment of the positively charged PDDA/ATP micro-droplets. In contrast, the protease K concentration in the external continuous water phase was ca. 35 nM.

In comparison, the FITC-dextran-containing proteinosomes exhibited low interfacial contrast when viewed in water by optical microscopy (Fig. 1d), although they were readily resolved by using fluorescence microscopy to image the entrapped fluorescent macromolecules (Fig. 1e). The proteinosomes were structurally stable, spherical, non-aggregated, and contained a uniform distribution of the encapsulated polysaccharide. Significantly, no leakage of the macromolecular cargo was observed over several weeks (Supplementary Fig. 3). The proteinosomes were typically 10 to 80 μm in diameter, which was considerably larger than the coacervate micro-droplets; thus, there was often a mismatch in size between the interacting target and killer protocells.

Fluorescence-activated cell sorting analysis of predatory behaviour. Fluorescence-activated cell sorting (FACS) was used to statistically characterize the behaviour of a synthetic protocell community comprising protease K-containing PDDA/ATP coacervate micro-droplets and FITC-dextran-encapsulated BSA-NH$_2$/PNIPAAm proteinosomes. Control experiments using single populations of the coacervate micro-droplets or proteinosomes gave two-dimensional (2D) dot-plots of forward-scattered (FSC) vs side-scattered light (SSC) that were readily distinguishable. Although both single populations displayed a wide range of FSC values consistent with polydisperse particle size distributions, the SSC values were significantly higher for the FITC-dextran-containing proteinosomes (Fig. 2a,b), presumably due to increased granularity. As a consequence, two distinct populations of protocells were clearly resolved in the 2D dot-plots obtained after mixing dispersions of the coacervate micro-droplets and proteinosomes (t = 0; number ratio 8 : 1, respectively) (Fig. 2c). Significantly, a similar FACS analysis on the mixed dispersions after 60 min revealed only a single protocell population that corresponded to coacervate micro-droplets with a slightly increased granularity (Fig. 2d). In contrast, two distinct populations of coacervate micro-droplets and proteinosomes were observed after mixing for 300 min in control experiments undertaken in the absence of protease K (Supplementary Fig. 4).

4

Moreover, incubation of a single population of FITC-dextran-containing proteinosomes in an aqueous solution of protease K at a concentration (35 nM) equivalent to the equilibrium value determined for the continuous phase of the coacervate dispersions did not induce proteinosome degradation (Supplementary Fig. 5). Taken together, these observations were consistent with an interacting community of positively and negatively charged protocells in which selective disassembly of the proteinosomes occurred by protease K-mediated lysis of the cross-linked BSA-PNIPAAm membrane building blocks on contact with the coacervate micro-droplets.

As expected, the fluorescence intensity distributions for single populations of the coacervate or proteinosome particles were markedly different due to encapsulation of FITC-dextran in the protein-polymer micro-compartments (Fig. 2e,f). Whilst the coacervate micro-droplets were essentially silent in terms of their fluorescence signal, the proteinosomes showed a wide range of intensities that were often several orders of magnitude greater than the background fluorescence observed in the PDDA/ATP micro-droplets. Interestingly, when mixed as a binary population with a coacervate micro-droplet : proteinosome number density ratio of approximately 8 : 1 , the histograms produced at t = 0 and 60 min showed significant changes in the frequency distribution for both components (Fig. 2g,h). Immediately after mixing, the FACS analysis of the gated populations identified in the 2D dot-plots showed two fluorescence intensity profiles with different ranges but similar values of the maximum peak intensity (Fig. 2g). Although the FITC-dextran-containing proteinosome population distribution was essentially unchanged, the histograms at t = 0 indicated that there was an approximately ten-fold increase in the mean fluorescence intensity associated with the coacervate micro-droplets, which was attributed to the sequestration of trace amounts of FITC-dextran present in the continuous phase of the proteinosome dispersion (Supplementary Fig. 6; control experiments). In contrast, only a single FITC fluorescence distribution was observed after protease-mediated lysis of the proteinosome membrane via interaction with the coacervate micro-droplets over a period of 60 min (Fig. 2h). Consistent with the 2D dot-plots (Fig. 2d), the surviving population was attributed to a dispersion of intact coacervate micro-droplets. However, the corresponding mean fluorescence intensity of the coacervate micro-droplets at t = 60 min was approximately ten times of that recorded at t = 0, and two orders of magnitude greater than the background fluorescence recorded for the coacervate population prior to mixing, suggesting that the FITC-dextran payload was effectively transferred from the proteinosomes to the enzyme-containing

coacervate micro-droplets during protease K-induced disassembly of the protein-polymer micro-compartments.

To investigate the details of the population dynamics associated with this artificial form of primitive predatory behaviour, we undertook time-dependent FACS experiments over the first 5 min period after preparation of the synthetic protocell community. Two distinct populations corresponding to the enzyme-containing coacervate micro-droplets and FITC-dextran-loaded proteinosomes at an initial number ratio of 2.5 : 1 (volume ratio 1 : 2.5) were observed throughout the first 5 min period after mixing (Supplementary Fig. 7). During the initial stages, the coacervate micro-droplet population remained essentially constant (Fig. 2i), whilst the proteinosome counts reduced linearly to approximately one-third of their initial value. The associated FITC intensity distributions were well resolved, with the gated coacervate and proteinosome particle populations displaying medium fluorescence intensities at values of approximately 10^3 and $10^{4.5}$, respectively (Fig. 2j and 2k, Supplementary Fig. 7). Moreover, the overall fluorescence intensity of the coacervate micro-droplets and proteinosome populations increased and decreased linearly over this period, respectively (Fig. 2l), as FITC-dextran was transferred between the protocells. Corresponding control experiments on the binary population prepared with protease-free coacervate micro-droplets showed only minimal changes in the time-dependent histogram profiles (Supplementary Fig. 8).

As contact between the positively charged coacervate micro-droplets and negatively charged proteinosomes was expected to depend not only on electrostatic interactions but also on the relative numbers of killer and target protocells in the synthetic community, we investigated the effect of changing the number of FITC-dextran-containing proteinosomes in a binary population containing a fixed number of coacervate micro-droplets. As shown in Supplementary Fig. 9, decreasing the initial coacervate micro-droplet : proteinosome particle numbers ratios from 30 : 1 to 6 : 1 to 0.5 : 1, decreased the rate of proteinosome killing observed during the initial 5 min. Indeed, hardly any decrease in the proteinosome population was observed during this initial time period at a number ratio of 0.5 : 1, indicating that the predatory behaviour was strongly dependent on the interaction probability within the synthetic protocell community.

Coacervate micro-droplet-mediated proteinosome disassembly and payload transfer. Given the above FACS observations on the population dynamics of mixed dispersions of protease K-

sequestered PDDA/ATP coacervate micro-droplets and FITC-dextran-encapsulated BSA-NH$_2$/PNIPAAm proteinosomes, we used optical and fluorescence microscopy to elucidate the mechanisms responsible for the apparent predatory behaviour in the synthetic protocell community. In general, identification of the different protocells in the binary population was facilitated by the relative high optical density and low (background) fluorescence of the enzyme-containing coacervate micro-droplets, combined with the low optical contrast and high fluorescence of the FITC-dextran-encapsulated proteinosomes.

The importance of electrostatic binding on the killing potential was confirmed by determining the number density of surviving proteinosomes before and 30 min after the addition of a dispersion of negatively charged proteinosomes to protease-containing coacervate micro-droplets prepared with positive (ζ = + 25 mV), close to neutral (ζ = + 2 mV) or negative (ζ = -21 mV) surface potentials (Supplementary Fig. 10). Optical microscopy was used to count the intact proteinosomes, and indicated that 98 ± 2% of the negatively charged proteinosomes were disassembled over 30 min in the presence of the positively charged coacervate micro-droplets. In contrast, addition of the neutral or negatively charged PDDA/ATP droplets gave rise to a killing potential of only 29 ± 17% and 21 ± 18%, respectively.

Electrostatically induced attachment of the positively charged, smaller coacervate killer micro-droplets onto the external surface of negatively charged single proteinosomes was observed within several minutes after *in situ* mixing of the two suspensions in the sample holder of an optical microscope (Fig. 3a-d). Significantly, both types of protocell remained intact on initial contact, and minimal wetting was observed. As a consequence, the coacervate micro-droplets were attached as discrete, spatially localized satellites that adopted a hemispherical morphology with an interfacial contact angle of between 70 and 95° (Supplementary Fig. 11). Corresponding fluorescence microscopy images clearly revealed the location of the FITC-dextran-loaded proteinosomes before and immediately after attachment of the protease K-containing coacervate micro-droplets, and indicated that the polysaccharide payload remained encapsulated within the intact proteinosomes (Fig. 3e-h).

Due to the relatively large size of the protein-polymer micro-compartments, multiple coacervate killer micro-droplets were initially attached to single target proteinosomes (Supplementary Fig. 12). Subsequent interactions between the conjoined protocells were monitored by optical microscopy, which showed that the proteinosome membrane was typically dismantled over a period of approximately 10-30 min (Fig. 3i-k; Supplementary Movie 1). Time-

dependent changes in the optical texture specifically at the contact points between the multiple coacervate micro-droplets attached to a single proteinosome indicated that lysis of the protein-polymer membrane occurred specifically at the attachment sites of the protease K-containing micro-droplets (Fig. 3i-k, arrows). As a consequence, the individual proteinosomes collapsed (Fig. 3i-k, circles) and became obliterated through the collective binding and enzymatic activity of the killer protocells. Corresponding fluorescence microscopy images of the killing process showed a progressive loss of the fluorescence intensity associated with the proteinosome micro-compartments (Fig. 3l,m, Supplementary Fig. 13; Supplementary Movie 2), consistent with release of encapsulated FITC-dextran. Moreover, the time-dependent images of the conjoined protocells and their associated fluorescence intensity line scans (Fig. 3n,o), indicated that the progressive loss of fluorescence intensity associated with the proteinosome micro-compartment was correlated with a corresponding increase in the fluorescence intensity of the attached coacervate micro-droplets, particularly at their exposed surfaces and contact points.

The above observations were attributed to coacervate micro-droplet-mediated release of the proteinosome-entrapped FITC-dextran via slow enzymatic digestion of the protein-based membrane and mass transfer of the negatively charged macromolecular payload partially from the target to the positively charged killer protocells at the contact interface between the two different protocells. Dismantling of the proteinosome membrane into peptide fragments resulted in the collapse of the micro-compartment and detachment of the coacervate killer micro-droplets, which re-adopted a spherical morphology, and remained enzymatically active towards small molecule substrates such as N-succinyl-L-phenylalanine *p*-nitroanilide (Supplementary Fig. 14). Moreover, addition of a new population of proteinosomes after the killing event gave rise to a second cycle of predatory behaviour, which was repeatable for at least 4 cycles, although the activity slowly decreased due to the progressive accumulation of membrane fragments and FITC-dextran on the surface of the coacervate micro-droplets (Supplementary Fig. 15). Furthermore, measurements of the zeta potential of the coacervate micro-droplets after obliteration of the proteinosome population showed a decrease in the surface charge from a pre-attack value of +25 mV to +5 mV (Supplementary Fig. 16). This was attributed to a change in the surface composition of the coacervate killer micro-droplets, as evidenced by various control experiments (Supplementary Fig. 17), as well as fluorescence microscopy images of the protease K-containing coacervate droplets after detachment from the disassembled proteinosomes. The images showed an intense ring of green fluorescence

associated specifically with the formation of a polysaccharide-rich spherical shell on the surface of the PDDA/ATP micro-compartments (Fig. 3p). Similar experiments involving binary populations of protease K-containing coacervate micro-droplets and FITC-dextran-loaded rhodamine B-labelled BSA-NH$_2$/PNIPAAm proteinosomes indicated that the surface of the dextran-coated killer protocells also comprised a relatively high concentration of peptide-polymer fragments after disintegration of the proteinosome target micro-compartments (Fig. 3q). Other analogous studies using protease K-containing coacervates prepared with a rhodamine B-labelled PDDA indicated that the dextran- and peptide-polymer-coated outer shell was produced without disruption of the enzyme-containing coacervate interior (Fig. 3r). We also undertook investigations to assess the influence of payload charge on macromolecular transfer into the positively charged killer protocells. For this, we prepared proteinosomes with encapsulated positively charged polysaccharides (RhITC-dextran or FITC-DEAE-dextran) in place of negatively charged FITC-dextran, and used fluorescence microscopy to assess the degree of macromolecular uptake after the killing event. The images indicated an absence of polysaccharide uptake in the protease-containing coacervate micro-droplets (Supplementary Fig. 18), suggesting that electrostatic interactions played an important role in facilitating the trafficking process.

DNA trafficking in binary protocell populations. Given the ability of the protease K-containing coacervate micro-droplets to act as artificial killer protocells for obliteration of a population of proteinosomes and subsequent transfer and capture of their polysaccharide payload, we investigated whether this synthetic predatory behaviour could be exploited for the trafficking of genetic information or functional components such as non-biological catalysts from one protocell type to another within a synthetic protocell community. As proof-of-principle, two distinct populations of negatively charged proteinosomes were prepared containing carboxyfluorescein (FAM)-modified *ss*-DNA (99 nucleotides, 5$^/$-linked, zeta potential *ca.* -18 mV) (**I**) or carboxytetramethylrhodamine (TAMRA)-tagged *ss*-DNA (99 nucleotides, 3$^/$-coupled, zeta potential *ca.* -16 mV) (**II**); in both cases, discrete micro-compartments exhibiting green or red fluorescence, respectively, were observed (Fig. 4a,b), indicating that the DNA payloads were retained in the protein-polymer micro-compartments after transfer into water.

Incubation of proteinosomes **I** or **II** with a population of protease K-containing PDDA/ATP coacervate micro-droplets resulted in lysis of the protein-polymer membrane and release of the

entrapped DNA molecules by a mechanism described above for FITC-dextran-containing proteinosomes. However, unlike the released FITC-dextran, the *ss*-DNA was homogeneously sequestered into the interior of the killer protocells rather than forming a discrete outer shell along with the peptide-polymer fragments (Fig. 4c). We attributed this to the high charge density of *ss*-DNA and relatively strong DNA/PDDA interactions, which facilitate penetration of the polynucleotide into the molecularly crowded coacervate interior.[22,24] Control experiments confirmed that *ss*-DNA and FITC-protease K were co-sequestered into the coacervate micro-droplet interior, and that RhITC-BSA-NH$_2$/PNIPAAm nanoconjugates and their enzyme-digested fragments were bound predominantly to the droplet surface (Supplementary Fig. 19). In contrast, optical fluorescence microscopy images of protease-free coacervate micro-droplets after incubation with the DNA-containing proteinosomes showed no detectable fluorescence indicating that the level of background leakage was very low (Supplementary Fig. 20).

To test whether it was possible to extract, transfer and capture different depositories of genetic information via protocell-protocell interactions, we mixed two individual populations of proteinosomes **I** or **II** with a suspension of protease K-containing coacervate micro-droplets, and exploited the Förster resonance energy transfer (FRET) behaviour associated with double-strand hybridization of the two covalently-labeled complementary *ss*-DNAs (i.e. FAM-*ss*-DNA/TAMRA-*ss*-DNA donor/acceptor pair) as a proxy for multiple killing events amongst proteinosomes carrying different polynucleotide cargos (Fig. 4d and Supplementary Fig. 21). Whereas fluorescence spectra recorded for coacervate micro-droplets analysed after disassembly and release of DNA from single populations of proteinosomes **I** or **II** showed characteristic emission peak maxima at 520 or 583 nm, respectively, spectra obtained when the killing process was applied to a mixed community of proteinosomes **I** and **II** indicated that the 520 and 583 nm peaks were quenched and increased, respectively (Fig. 4e), consistent with FRET pairing of the covalently-labeled dye molecules associated with double-strand formation of the complementary *ss*-DNAs. In contrast, control experiments in which protease K-free coacervate micro-droplets were used in combination with a mixed population of proteinosomes containing either FAM-*ss*-DNA or TAMRA-*ss*-DNA showed minimal spectroscopic evidence for FRET pairing, indicating that background leakage from the proteinosomes was negligible (Fig. 4e). The spectroscopic data was consistent with fluorescence microscopy studies of the enzyme-containing micro-droplets recorded after dismantling proteinosomes **I** or **II**, which showed weak green and red fluorescence in the filtered images, as well as a yellow coloration (red/green mix)

in the superimposed images (Fig. 4f-h). Significantly, control experiments with mixed populations of protease K-containing coacervate micro-droplets containing FAM-*ss*-DNA or TAMRA-*ss*-DNA showed no FRET response (Supplementary Fig. 22), suggesting that exchange of the oligonucleotides through the continuous aqueous phase was negligible. Thus, taken together the above results were consistent with multiple killing of a mixed community of proteinosomes followed by direct capture of their different types of encapsulated genetic information by a roaming population of protease K-containing coacervate micro-droplets.

Platinum nanoparticle transfer and catalytic modification of coacervate micro-droplet killer protocells. Based on the above results, we also investigated whether it was possible to extract, transfer and capture catalytic inorganic nanoparticles from the proteinosomes using the protease K-containing PDDA/ATP coacervate micro-droplets, such that the killer protocells adopt new catalytic properties. As an example of this strategy, we prepared negatively charged proteinosomes containing encapsulated platinum (Pt) nanoparticles, subjected this population to enzyme-mediated membrane degradation by attachment of positively charged protease K-containing coacervate micro-droplets, and then assayed the killer protocells for Pt nanoparticle-mediated catalytic activity (Fig. 5a). In this regard, our aim was to strongly sequester a small-molecule substrate within the coacervate micro-droplets so that the system remains dormant in the presence of the Pt nanoparticle-loaded proteinosomes unless the killing process occurs and the inorganic catalyst is released and partitioned into the coacervate-based protocells.

As the Pt nanoparticles were 5-15 nm in size (Supplementary Fig. 23) and non-fluorescent, we used transmission electron microscopy (TEM) and energy dispersive X-ray analysis (EDXA) to track their spatial location before and after the killing process. Significantly, the negatively charged Pt nanoparticles (zeta potential, -25.2 mV, Supplementary Fig. 23) were released from the proteinosomes and transferred and captured in the positively charged protease K-containing coacervate micro-compartments (Fig. 5b,c, and Supplementary Fig. 24). As a consequence, pre-sequestration of Amplex red (K = [Amplex red]$_{in}$/[Amplex red]$_{out}$ ≈ 900), along with protease K in the coacervate protocells gave rise to Pt nanoparticle-mediated peroxidase-like activity specifically in the PDDA/ATP micro-droplets, which exhibited a uniform red fluorescence due to the formation of resorufin (Fig. 5d and Supplementary Fig. 25). In contrast, addition of hydrogen peroxide to a binary population of protease K-free Amplex red-containing coacervate micro-droplets and Pt nanoparticle-loaded proteinosomes showed no change in fluorescence intensity

in the absence of membrane lysis (Fig. 5d). Additional experiments indicated that the transferred Pt nanoparticles could be used to generate coacervate-based protocells capable of oxygen bubble generation (Supplementary Fig. 26), and that alternative inorganic nanostructures such as 12 nm-sized negatively charged (zeta potential, -17 mV) gold nanoparticles could be accessed, transferred and captured by the coacervate killer micro-droplets using the above strategies (Supplementary Fig. 27-29).

Conclusions

In this paper, we demonstrate that a binary population of positively charged protease K-sequestered PDDA/ATP coacervate micro-droplets and negatively charged BSA-NH$_2$/PNIPAAm proteinosomes containing FITC-labeled dextran, *ss*-DNAs or platinum nanoparticles functions as an interacting system of compartmentalized colloidal objects that represent a synthetic protocell community capable of displaying a simple form of predatory behaviour. The population dynamics inherent in this consortium were monitored by FACS, which revealed a progressive loss of the targeted proteinosome population over a period of approximately 60 min depending on the coacervate micro-droplet : proteinosome number ratio. Obliteration of the proteinosome population occurred via electrostatic attachment of the two types of protocells, followed by highly localized protease-induced disassembly of the protein-polymer membrane and subsequent release of the killer coacervate micro-droplets. Significantly, slow enzymatic digestion of the protein-based membrane was associated with extraction, transfer and capture of the proteinosome payload to produce a population of compositionally and structurally modified coacervate micro-droplets. As a consequence, the artificial predatory behaviour can be used for the trafficking of genetic information or non-biological catalysts between the different protocell types in the community.

In general, our results illustrate an approach to the design of synthetic protocell communities capable of novel collective and emergent behaviour, and provide a step towards the use of compartmentalized colloidal objects as interacting functional systems. A focus towards developing protocell consortia should offer new directions for the development of complex functional micro-systems based on dispersed rather than integrated functionalities, and stimulate a path towards the notion of *protocell ecosystems*. In so doing, concepts such as specialization ("division of labour"), cooperation, competition, signalling, communication, symbiosis and predation could play an important role in bridging the gap between biology and

materials science, and advancing the development of new synthetic constructs and systems with life-like emergent properties and behaviours.

Methods

Preparation of protocells. Synthesis of BSA-NH$_2$/PNIPAAm nano-conjugates and assembly into negatively charged proteinosomes dispersed in water were undertaken as described previously.[18] Proteinosomes comprising encapsulated FITC-dextran (5.0 mg/mL; M$_w$ = 70,000), alkaline phosphatase (ALP, 10.0 mg/mL) or dsDNA (5.0 mg/mL, bp ~ 2000, Mw ~1300 kDa; stained by SYBR green I (1000 times diluted in water)) were prepared using similar methods (see Supplementary Methods). Enzyme-containing coacervate micro-droplets were prepared at room temperature and pH 8.0 by centrifugation and redispersion of a mixture of poly(diallyldimethylammonium chloride) (PDDA, M$_w$ = 100-200 kDa), protease K (*Tritirachium album*, 28.93 kDa), and adenosine 5$^/$-triphosphate (ATP) as described elsewhere[19] (see Supplementary Methods).

Fluorescence-activated cell sorting (FACS) analysis. Dispersions (ca. 1 mL) of protease K-containing PDDA/ATP coacervate micro-droplets, FITC-dextran-encapsulated proteinosomes, or mixed coacervate/proteinosome populations prepared at coacervate: proteinosome number ratios of 30 : 1, 8 : 1, 6 : 1, 2.5 : 1 and 0.5 : 1 were investigated by fluorescence-activated cell sorting (FACS) using a FACS Canto II flow cytometer operating at low pressure with a 100 µm sorting nozzle. 2D dot-plots of the forward- (FSC) and side-scattered (SSC) light were determined for a total of 20,000 particles in the single or binary populations. 2D dot-plots were also recorded for the coacervate/proteinosome dispersions at various time periods after mixing the two populations. Given the processing time required to collect the FACS data, the first measured dot-plot (*t* = 0) was typically recorded after 50 s. Count data for the membrane-free coacervate micro-droplets often varied between different control experiments due to the sensitivity of the particles to movement in the flow system of the cytometer. In contrast, the membrane-bounded proteinosomes were considerably more stable as control suspensions when investigated by FACS. The fluorescence intensity of individual particles was monitored by excitation and detection with a 488 nm blue laser and a 530 ± 30 nm filter, respectively. Histograms of the number of counts for gated populations of proteinosomes or coacervates against their corresponding fluorescence intensity (FITC-A) at different time points after mixing were determined. Data analysis was performed with FlowJo 7.6 software.

Optical and confocal fluorescence microscopy studies on interacting protocells. Dispersions of protease K-containing PDDA/ATP coacervate micro-droplets or FITC-dextran-encapsulated proteinosomes were introduced from separate ends of a homemade sample cell (Supplementary Fig. S30), and allowed to slowly mix under the optical field of view. Typically, 20 µL of the suspensions were loaded into a PEGsilane-functionalized capillary slide. Time-dependent optical and fluorescence images were recorded on the interacting protocells using a Leica inverted microscope DMI3000B with an immersion oil 100x lens. Fluorophores were excited by using specific filters with the following excitation (λ$_{ex}$) and emission wavelength cut offs (λ$_{em}$); FITC, λ$_{ex}$ = 450 - 490 nm, cut off 510 nm; RhITC, λ$_{ex}$ = 515 - 560 nm, cut off 580 nm; Hoechst 33342, λ$_{ex}$ = 355 - 425 nm, cut off 455 nm. Image analysis was performed with Image J software.

DNA transfer via coacervate micro-droplet-mediated proteinosome disassembly. Dispersions (*ca.* 50 μL) of protease K-containing PDDA/ATP coacervate micro-droplets and FAM-*ss*-DNA-containing proteinosomes (**I**) were mixed at a number ratio of 2.5 : 1, and the artificial predatory behavior was investigated by optical and confocal fluorescence microcopy. Similar killing experiments were performed on binary populations of protease K-containing PDDA/ATP coacervate micro-droplets and TAMRA-*ss*-DNA-containing proteinosomes (**II**). Fluorophores were excited in the microscopy experiments by using specific filters with the following excitation (λ_{ex}) and emission wavelength cut offs (λ_{em}); FAM-*ss*-DNA, λ_{ex} = 476 nm, cut off 500 nm; TAMRA-*ss*-DNA, λ_{ex} = 514 nm, cut off 550 nm. Förster resonance energy transfer (FRET) was quantified by measuring the fluorescence emission from FAM-*ss*-DNA and TAMRA-*ss*-DNA on a fluorometer (see Supplementary Methods).To test whether multiple transfers could be achieved during the killing process, two individual populations of proteinosomes **I** and **II** at a number ratio of 1 : 1 were mixed with a suspension of protease K-containing coacervate micro-droplets to give a coacervate micro-droplet : total proteinosome number ratio of 2.5:1.

Platinum nanoparticle-mediated peroxidase activity in coacervate killer protocells. Amplex Red was sequestered into protease K-containing coacervate micro-droplets, and the dispersion then added to a suspension of Pt nanoparticle-encapsulated proteinosomes such that extraction, transfer and capture of the Pt catalyst promoted the oxidation of Amplex Red (red fluorescent) within the killer protocells in the presence of added hydrogen peroxide. See Supplementary Methods for further details.

References

1   Huang, X., Patil, A. J., Li, M. & Mann, S. Design and construction of higher-order structure and function in proteinosome-based protocells. *J. Am. Chem. Soc.* **136**, 9225-9234 (2014).
2   Renggli, K. *et al.* Selective and responsive nanoreactors. *Adv. Funct. Mater.* **21**, 1241-1259 (2011).
3   Städler, B. *et al.* Polymer hydrogel capsules: en route toward synthetic cellular systems. *Nanoscale* **1**, 68-73 (2009).
4   Caschera, F. & Noireaux, V. Integration of biological parts toward the synthesis of a minimal cell. *Curr. Opin. Chem. Biol.* **22**, 85-91 (2014)
5   Li, M., Huang, X., Tang, T. Y. D. & Mann, S. Synthetic cellularity based on non-lipid micro-compartments and protocell models. *Curr. Opin. Chem. Biol.* **22**, 1-11 (2014).
6   Miller, D. M. & Gulbis, J. M. Engineering protocells: prospects for self-assembly and nanoscale production-lines. *Life* **5**, 1019-1053 (2015).
7   Nourian, Z. & Danelon, C. Linking genotype and phenotype in protein synthesizing liposomes with external supply of resources. *ACS Synth. Biol.* **2**, 186-193 (2013).
8   Martini, L. & Mansy, S. S. Cell-like systems with riboswitch controlled gene expression. *Chem. Commun.* **47**, 10734-10736 (2011).
9   Peters, R. J. *et al.* Cascade reactions in multicompartmentalized polymersomes. *Angew. Chem. Int. Ed.* **53**, 146-150 (2014).
10 Peters, R. J. R. W., Louzao, I. & van Hest, J. C. M. From polymeric nanoreactors to artificial organelles. *Chem. Sci.* **3**, 335-342 (2012)
11 Keating, C. D. Aqueous phase separation as a possible route to compartmentalization of biological molecules. *Acc. Chem. Res.* **45**, 2114-2124 (2012).
12 Dominak, L. M., Omiatek, D. M., Gundermann, E. L., Heien, M. L. & Keating, C. D. Polymeric crowding agents improve passive biomacromolecule encapsulation in lipid vesicles. *Langmuir* **26**, 13195-13200 (2010).
13 Chandrawati, R. & Caruso, F. Biomimetic liposome- and polymersome-based multicompartmentalized assemblies. *Langmuir* **28**, 13798-13807 (2012).
14 Chandrawati, R. *et al.* Engineering advanced capsosomes: maximizing the number of subcompartments, cargo retention, and temperature-triggered reaction. *ACS Nano* **4**, 1351-1361 (2010).
15 Torre, P., Keating, C. D. & Mansy, S. S. Aqueous multi-phase systems within water-in-oil emulsion droplets for the construction of genetically encoded cellular mimics. *Langmuir*, **30**, 5695-5699 (2014).
16 Tawfik, D.S. & Griffiths, A.D. Man-made cell-like compartments for molecular evolution. *Nature Biotechn.* **16**, 652-656 (1998).
17 Li, M., Harbron, R. L., Weaver, J. V. M., Binks, B. P. & Mann, S. Electrostatically gated membrane permeability in inorganic protocells. *Nature Chem.* **5**, 529-536 (2013).
18 Huang, X. *et al.* Interfacial assembly of protein-polymer nano-conjugates into stimulus-responsive biomimetic protocells. *Nature Commun.* **4**, 2239 (2013).
19 Koga, S., Williams, D. S., Perriman, A. W. & Mann, S. Peptide-nucleotide microdroplets as a step towards a membrane-free protocell model. *Nature Chem.* **3**, 720-724 (2011).
20 Fothergill, J., Li, M., Davis, S. A., Cunningham, J. A. & Mann, S. Nanoparticle-based membrane assembly and silicification in coacervate microdroplets as a route to complex colloidosomes. *Langmuir* **30**, 14591-14596 (2014).
21 Williams, D. S., Patil, A. J. & Mann, S. Spontaneous structuration in coacervate-based protocells by polyoxometalate-mediated membrane assembly. *Small* **10**, 1830-1840 (2014).
22 Tang, T. Y. D. *et al.* Fatty acid membrane assembly on coacervate microdroplets as a step towards a hybrid protocell model. *Nature Chem.* **6**, 527-533 (2014).
23 Huang, X., Li, M. & Mann S. Membrane-mediated cascade reactions in enzyme-polymer proteinosomes. *Chem. Commun.* **50**, 6278-6280 (2014).
24 van Swaay D., Tang T-Y D., Mann S., & deMello A. Microfluidic formation of membrane-free aqueous coacervate droplets in water. *Angew. Chem. Int. Ed.* **54,** 8398-401 (2015).
25 Tang, T-Y D., van Swaay, D., deMello, A., Anderson, J. L R., & Mann, S. *In vitro* gene expression within membrane-free coacervate protocells. *Chem. Commun.* **51**, 11429-11432 (2015).
26 Crosby, J. *et al.* Stabilization and enhanced reactivity of actinorhodin polyketide synthase minimal complex in polymer/nucleotide coacervate droplets. *Chem. Commun.* **48**, 11832-11834 (2012).

27   Yin Y. *et al*. Electric field excitation and non-equilibrium dynamics in polypeptide/DNA synthetic protocells. *Nature Commun.* **7**, 10658 (2016).

28   Stano, P. & Luisi, P. L. Semi-Synthetic Minimal Cells: Origin and Recent Developments. *Curr. Opin. Biotechnol.* **24**, 633-638 (2013).

29   Goff, L. L. & Lecuit, T. Phase Transition in a Cell. *Science* **324**, 1654-1655 (2009).

30   Hammer, D. A. & Kamat, N. P. Towards an Artificial Cell. *FEBS letters* **586**, 2882-2890 (2012).

31   Pohorille, A. & Deamer, D. Artificial Cells: Prospects for Biotechnology. *Trends in Biotech.* **20**, 123-128 (2002).

32   Gardner P. M., Winzer, K. & Davis, B. G. Sugar synthesis in a protocellular model leads to a cell signalling response in bacteria. *Nature Chem.* **1**, 377-383 (2009).

33   R. Lentini, *et. al.* Integrating artificial with natural cells to translate chemical messages that direct *E. coli* behaviour. *Nature Commun.* **5**, 4012 (2014).

34   Weitz M. *et al*. Diversity in the dynamical behaviour of a compartmentalized programmable biochemical oscillator, *Nature Chem.* **6**, 295–302 (2014).

35   Schwarz-Schilling, M., Aufinger, L., Muckl, A & Simmel, F. C. Chemical communication between bacteria and cell-free gene expression systems within linear chains of emulsion droplets. *Integrative Biology,* **8,** 564-570 (2016).

36.   Sun, S. *et. al.* Chemical Signaling and Functional Activation in Colloidosome-Based Protocells. *Small,* **12**, 1920–1927 (2016).

37.   Rollie, S., Mangold, M. & Sundmacher, K. Designing biological systems: systems engineering meets synthetic biology. *Chem. Eng. Sci.* **69**, 1-29 (2012).

Author contributions: YQ, ML, SM conceived the experiments; YQ and RB performed the experiments; YQ and ML undertook the data analysis; YQ, ML, SM wrote the manuscript.

Competing financial interests
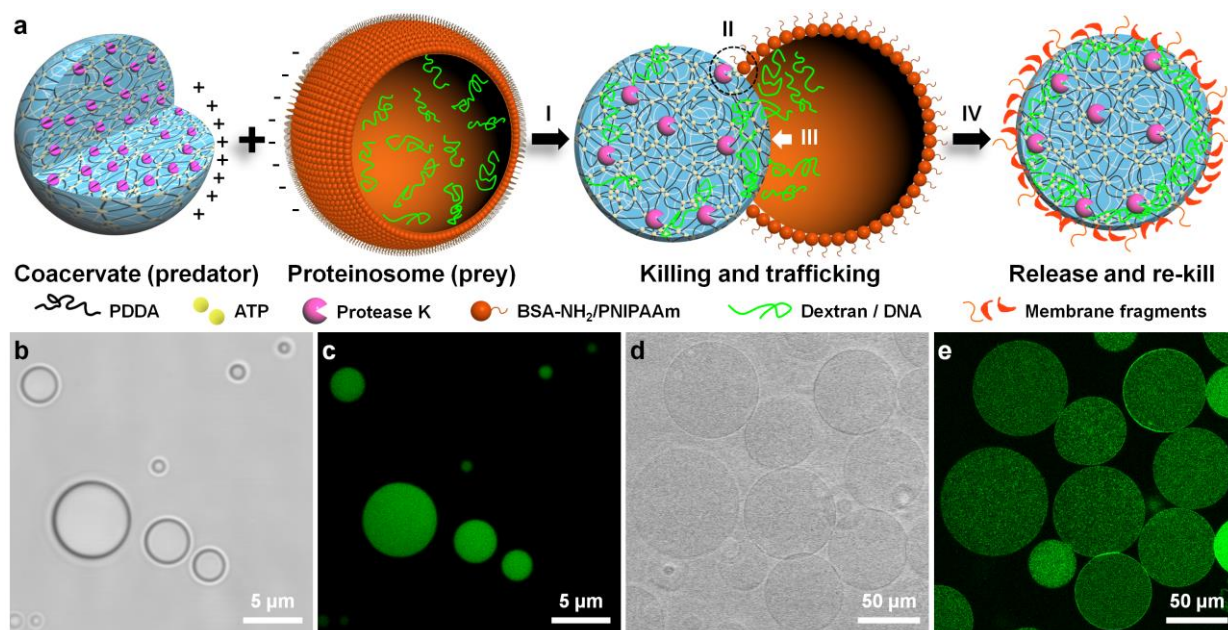The authors declare no competing financial interests.

Figure 1. Design and construction of a predator/prey synthetic protocell community. (**a**) Scheme showing overall strategy in which protease K-containing coacervate micro-droplets act as artificial killer protocells for the obliteration of a population of target proteinosomes and subsequent transfer and capture of their polysaccharide or *ss*-DNA payload. Four stages are envisioned: **I**, electrostatic attachment; **II**, protease-induced disassembly; **III**, payload transfer; and **IV**, release of the compositionally modified killer protocell. The protease-K-containing PDDA/ATP coacervate micro-droplets are positively charged, molecularly crowded, and comprise chemically enriched interiors. They are prepared by electrostatically mediated complexation in water, which leads to partial charge neutralization and liquid-liquid microphase separation.[19] The ATP is involved as a complexing anion and not utilized as an energy-dependent molecule. The proteinosomes are negatively charged and consist of a closely packed, cross-linked monolayer of conjugated globular protein-polymer building blocks. The nanoconjugate building blocks are synthesized by covalent coupling of approximately three molecules of PNIPAAm to the surface primary amine groups of a cationized form of bovine serum albumin (BSA-NH$_2$) to produce amphiphilic BSA-NH$_2$/PNIPAAm constructs that self-assemble around water-in-oil emulsion droplets containing dextran or *ss*-DNA. Crosslinking the BSA-NH$_2$/PNIPAAm membrane produces a semi-permeable, elastic shell, and facilitates transfer into water with retention of protein function.[18] (**b-e**) Optical (**b,d**) and fluorescence (**c,e**) microscopy images of FITC-labeled protease-containing coacervate micro-droplets (**b,c**), and FITC-dextran-encapsulated proteinosomes (**d,e**). Note the high and low interfacial contrast for the killer and target protocells, respectively, and presence of homogeneous green fluorescence from FITC-tagged molecules sequestered or encapsulated within the coacervate micro-droplets or proteinosomes, respectively.
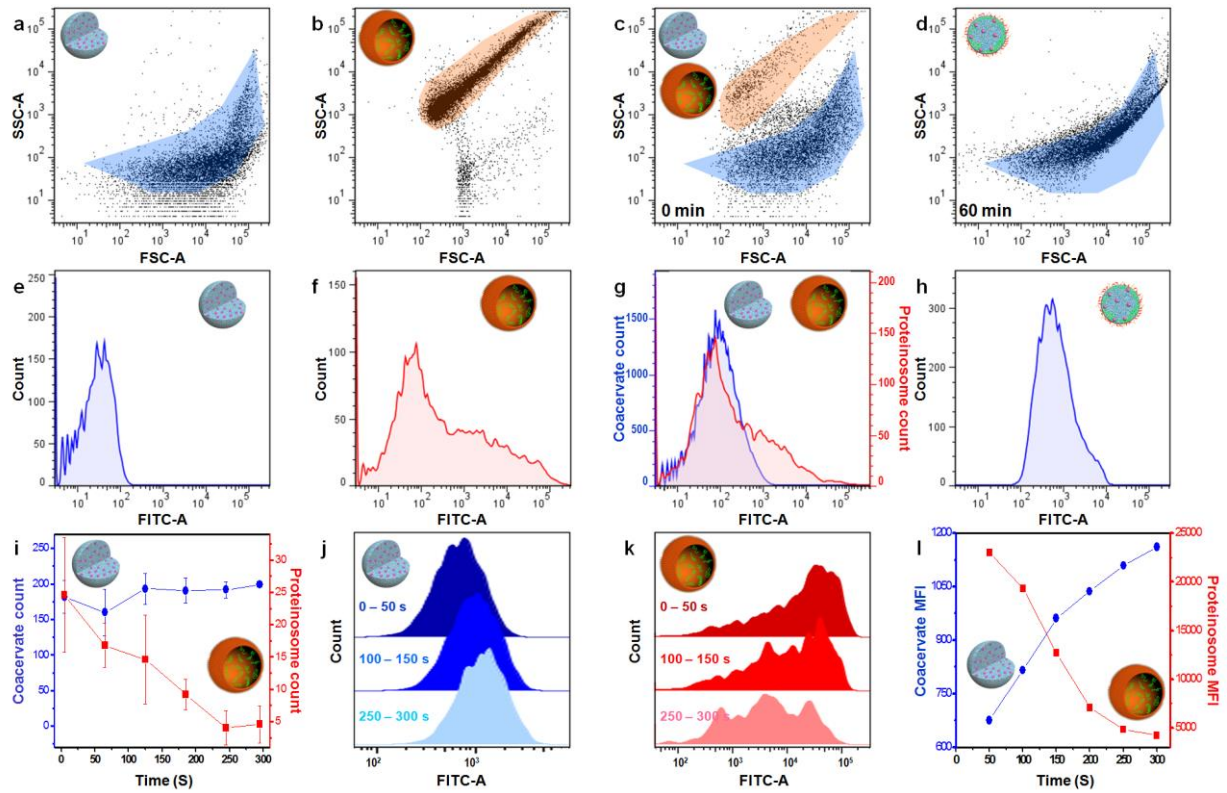
Figure 2. FACS analysis of predatory behavior in binary protocell populations. (**a-d**) 2D dot-plots of forward-scattered (FSC) *vs* side-scattered light (SSC) for protease K-containing coacervate micro-droplets (**a**), FITC-dextran-encapsulated proteinosomes (**b**), binary mixture immediately after mixing (*t* = 0 min; total particles = 20,000, coacervate droplet : proteinosome number ratio = 8 : 1) showing coexistence of coacervate micro-droplets (blue domain) and proteinosomes (red domain) (**c**), and binary population 60 min after mixing showing obliteration of the proteinosomes from the community (**d**). (**e-h**) Corresponding histograms of FITC fluorescence intensity (FITC-A) for samples shown in (**a-d**). See Supplementary Tables 1 and 2 for further quantitative analysis. (**i**) Plot of time-dependent changes in counts over an initial period of 5 min for coacervate micro-droplets (blue) and proteinosomes (red) showing constant and decreasing levels in the respective protocell populations. Counts were determined from the corresponding 2D dot-plots, averaged every 5 s and the standard deviation was calculated accordingly. (**j,k**) Time-dependent FACS-derived histograms for a binary population showing increase of FITC fluorescence intensity (FITC-A) for protease-containing coacervate micro-droplets (**j**) and correlated decrease in fluorescence for the FITC-dextran containing proteinosomes (**k**) after mixing for up to 5 min. (**l**) Time-dependent mean fluorescent intensity (MFI) plots of protease K-containing coacervate micro-droplets (blue) and FITC-dextran-encapsulated proteinosomes (red) in an interacting mixed population. Coacervate micro-droplet : proteinosome number ratio was 2.5 : 1 in (**i-l**).
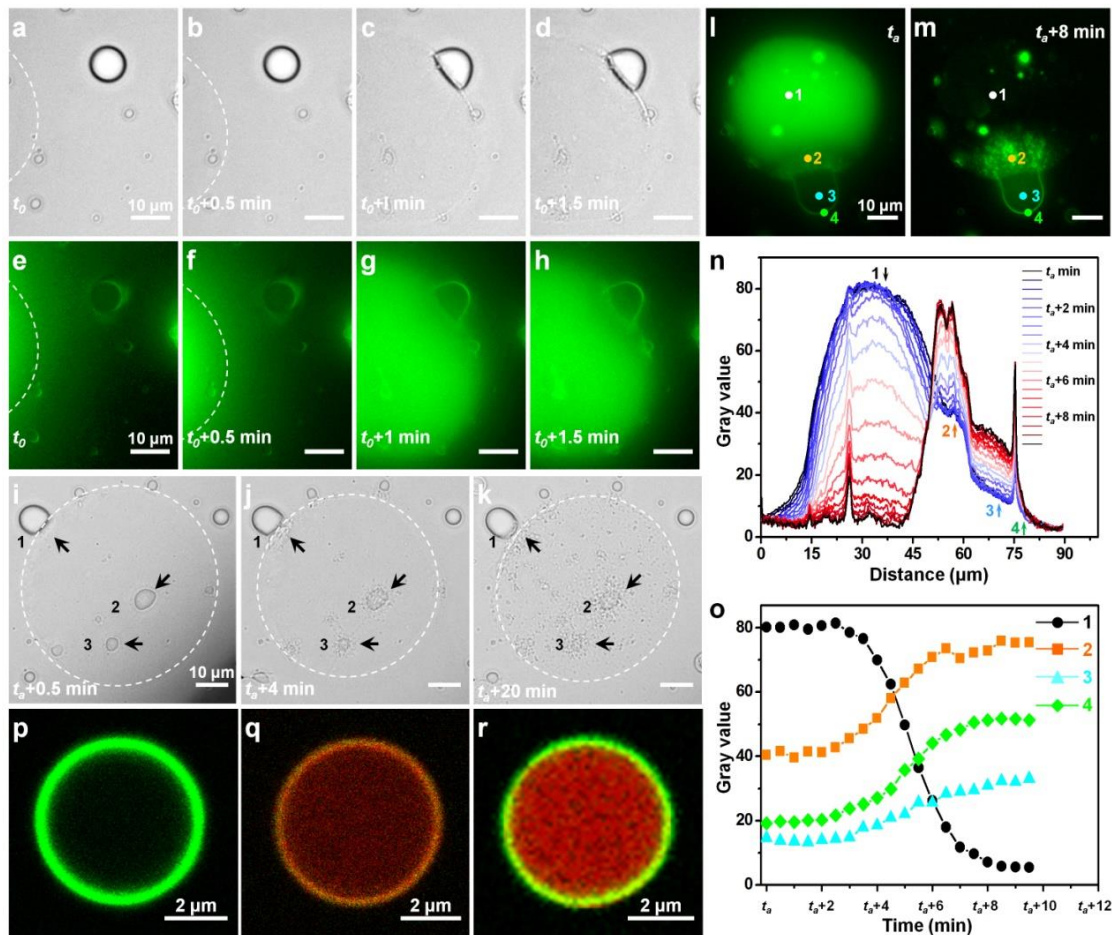
Figure 3. Coacervate micro-droplet-mediated proteinosome disassembly and payload transfer. (**a-d**) Time series of optical microscopy images showing approach of a single FITC-dextran-encapsulated BSA-NH$_2$/PNIPAAm proteinosome (dashed curve in (**a**)) towards an individual protease K-containing PDDA/ATP coacervate micro-droplet (**a,b**), followed by electrostatically induced attachment of the micro-droplet onto the outer surface of the proteinosome (**c,d**); scale bars, 10 μm. (**e-h**) Fluorescence microscopy images corresponding to (**a-d**), respectively; scale bars, 10 μm. (**i-k**) Time sequence of optical microscopy images showing stages of coacervate micro-droplet-mediated lysis of a single proteinosome at various times after attachment (time t_a). White circles delineate the proteinosome membrane, which collapses over time. Locations **1**, **2** and **3** indicate three attached coacervate micro-droplets, and white arrows highlight changes in optical texture associated with localized membrane disassembly; scale bars, 10 μm. See Supplementary Movie 1. (**l,m**) Fluorescence microscopy images showing time-dependent coacervate droplet-mediated release of FITC-dextran from a single proteinosome; scale bar = 10 μm. See Supplementary Movie 2. Numbering refers to locations used for line scanning of fluorescence intensities). (**n,o**) Time- and spatial-dependent changes in the fluorescence profiles (**n**), and relative fluorescence peak intensities (**o**), for the conjoined protocells shown in (**l,m**), and monitored inside the target proteinosome (**1**); at the contact interface (**2**); inside the attached coacervate micro-droplet (**3**); and at the exposed surface of coacervate micro-droplet (**4**). (**p-r**) Fluorescence microscopy images of single protease K-containing coacervate micro-droplets after detachment from disassembled FITC-dextran-loaded proteinosomes showing green fluorescent FITC-dextran shell arising from payload transfer (**p**), red fluorescent ring due to surface adsorption of peptide-polymer fragments of the digested rhodamine B-labelled BSA-NH$_2$/PNIPAAm membrane, overlaid with a green FITC-dextran ring (**q**), and homogeneous coacervate interior (red fluorescent rhodamine B-labelled PDDA) surrounded by a discrete FITC-dextran shell (green) (**r**); scale bars = 2 μm.
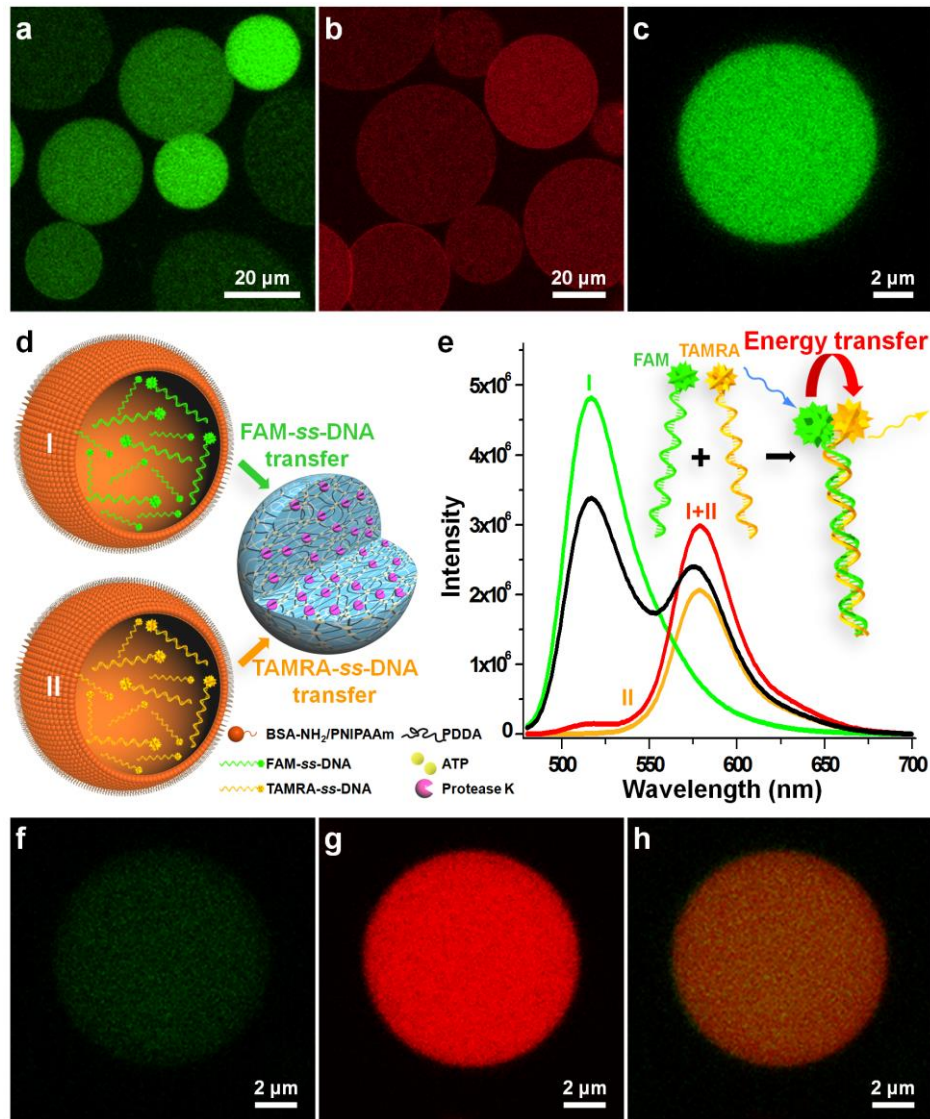
19

Figure 4. DNA trafficking in binary protocell populations. (**a,b**) Fluorescence microscopy images of water-dispersed cross-linked BSA-NH$_2$/PNIPAAm proteinosomes with encapsulated FAM-*ss*-DNA (**I**) (**a**), or TAMRA-*ss*-DNA (**II**) (**b**), payloads; scale bars, 20 μm. (**c**) Fluorescence microscopy image of a single protease K-containing PDDA/ATP coacervate micro-droplet recorded after disintegration of proteinosomes containing (**I**) showing transfer of green fluorescence to the killer protocell; scale bar, 2 μm. (**d**) Scheme showing coacervate micro-droplet-based multiple killing within a mixed community of proteinosomes loaded with the FRET partners **I** or **II**. (**e**) Fluorescence emission spectra recorded on dispersions of protease K-containing coacervate micro-droplets after enzyme-mediated disintegration of single populations of proteinosomes containing **I** (green plot), or **II** (orange plot), or after disassembly of a mixed population of these proteinosome (**I** + **II**) (red plot). The latter shows the presence of FRET pairing (inset) within the coacervate micro-droplets. Black plot shows control experiment involving protease K-free coacervate micro-droplets in combination with a mixed population of proteinosomes **I** and **II;** minimal FRET pairing is observed. (**f-h**) Fluorescence microscopy images of green (**f**) and red (**g**) filtered images, and green/red superimposed image (**h**) of protease K-containing coacervate micro-droplets after enzyme-mediated disassembly of a mixed population of proteinosomes **I** or **II**, showing presence of both types of DNA in the killer protocells and after FRET quenching of FAM-*ss*-DNA by TAMRA-*ss*-DNA; scale bars, 2 μm.
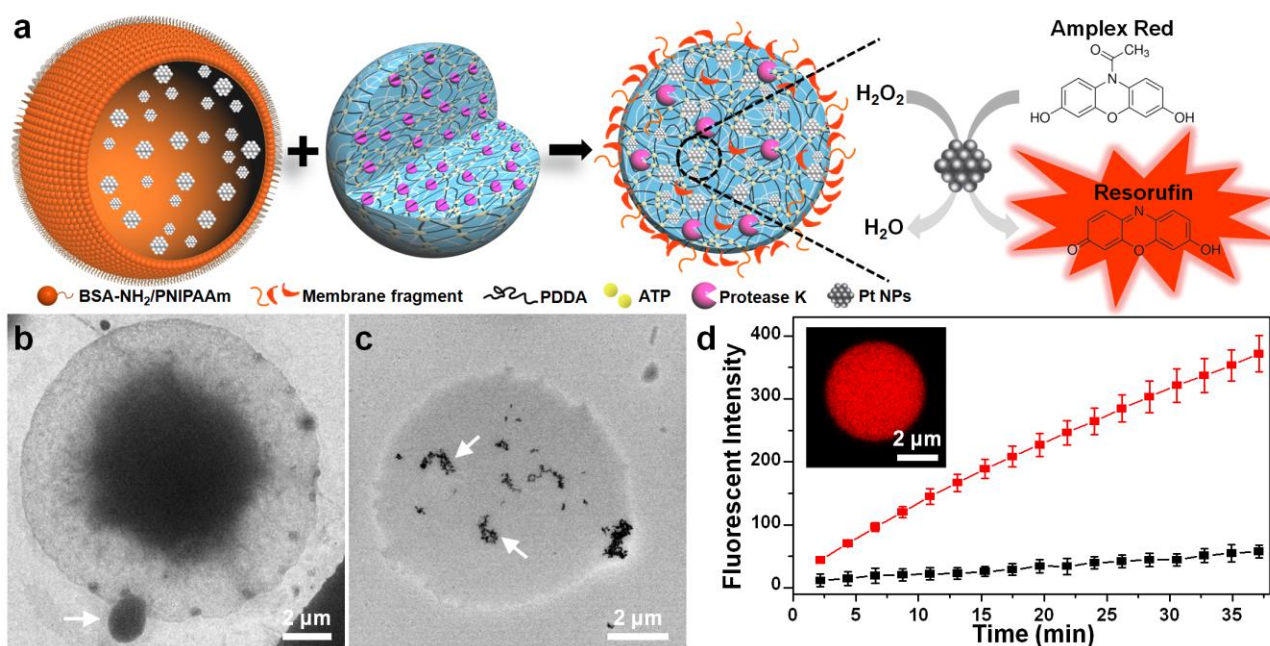
Figure 5. (a-d) Extraction, transfer and capture of inorganic catalysts by coacervate micro-droplet-mediated proteinosome disassembly. (**a**) Scheme showing protease K-containing coacervate micro-droplet-based disintegration of proteinosomes containing an aqueous dispersion of Pt nanoparticles, followed by transfer and capture of the inorganic catalysts to produce killer protocells with artificial peroxidase activity as demonstrated by the H_2O_2-mediated catalytic oxidation of Amplex Red to the fluorescent product resorufin. (**b**) TEM image of a single intact proteinosome containing encapsulated electron dense Pt nanoparticles; the sample was prepared approximately 1 min after mixing with a population of protease K-containing coacervate micro-droplets. Attachment of an individual killer protocells is highlighted (white arrow); scale bar, 2 μm. (**c**) TEM image showing single coacervate micro-droplet after enzyme-mediated disassembly of Pt nanoparticle-containing proteinosomes showing capture of the released electron dense Pt aggregates (white arrows) by the killer protocells. (**d**) Plot showing time-dependent increase in red fluorescence for a dispersion of Amplex red/protease K-containing PDDA/ATP micro-droplets after coacervate-mediated disintegration of Pt nanoparticle-loaded proteinosomes (red line). Catalytic oxidation of Amplex red to resorufin was initiated by addition of 0.1 mM H_2O_2. Similar experiments using dispersions of Amplex red-containing enzyme-free coacervate micro-droplets and intact Pt-nanoparticle-loaded proteinosomes showed no increase in red fluorescence (black line). No increase in red fluorescence was also observed for control experiments involving protease K-containing coacervate micro-droplets and Pt nanoparticle-free proteinosomes, or protease K-containing coacervate micro-droplets alone (Supplementary Fig. 23). Error bars indicate the standard deviation of three replicating measurements. Catalytic oxidation of Amplex red to resorufin produces red fluorescent killer protocells (inset), and is observed only when Pt nanoparticles are transferred to the coacervate micro-droplets via enzyme-mediated proteinosome membrane disassembly.

Online Legends for Movies

Movie 1. Optical microscopy video showing coacervate micro-droplet-mediated lysis of a single proteinosome. Movie is shown at x150 of real-time speed at 5 frames per second. Total duration of recording was 15 minutes in real time.

Movie 2. Fluorescence microscopy (left panel) and corresponding optical microscopy (right panel) videos showing coacervate micro-droplet-mediated release of FITC-dextran from a single proteinosome Movies are shown at x60 of real time speed at 2 frames per second. Total duration of recording was 10 minutes in real time.